HHS Public Access

Author manuscript

*Addit Manuf*. Author manuscript; available in PMC 2022 October 01.

Published in final edited form as:

*Addit Manuf*. 2022 October ; 46: . doi:10.1016/j.addma.2021.102097.

# Heat Transfer-Based Non-isothermal Healing Model for the Interfacial Bonding Strength of Fused Filament Fabricated Polyetheretherketone

**Cemile Basgul**[1], **Florian M. Thieringer**[2,3], **Steven M. Kurtz**[1,4]

[1]Implant Research Center, School of Biomedical Engineering, Science and Health Systems, Drexel University, Philadelphia, PA

[2]Medical Additive Manufacturing Research Group (Swiss MAM), Department of Biomedical Engineering, University of Basel, Allschwil, Switzerland

[3]Department of Oral and Cranio-Maxillofacial Surgery, University Hospital Basel, Basel, Switzerland

[4]Exponent, Inc., Philadelphia, PA

## Abstract

Fused Filament Fabrication (FFF) as an Additive Manufacturing (AM) method for Polyetheretherketone (PEEK) has established a promising future for medical applications so far, however interlayer delamination as a failure mechanism for FFF implants has raised critical concerns. A one-dimensional (1D) heat transfer model (HTM) was developed to compute the layer and interlayer temperatures by considering the nature of 3D printing for FFF PEEK builds. The HTM was then coupled with a non-isothermal healing model to predict the interlayer strength through thickness of a FFF PEEK part. We then conducted a parametric study of the primary temperature effects of the FFF system, including the print bed, nozzle, and chamber temperatures, on layer healing. The heat transfer component of the model for the FFF PEEK layer healing assessment was validated separately. An idealized PEEK cube design (10x10x10 $mm^3$) was used for model development and 3D printed in commercially available industrial and medical FFF machines. During the printing and cooling processes of FFF, thermal videos were recorded in both printers using a calibrated infrared camera. Thermal images were then processed to obtain time-dependent layer temperature profiles of FFF PEEK prints. Both the theoretical model and experiments confirmed that the upper layers in reference to the print bed exhibited higher temperatures, thus higher healing degrees than the lower layers. Increasing the print bed temperature increased the healing of the layers allowing more layers to heal 100%. The nozzle temperature showed the most significant effect on the layer healing, and under certain nozzle temperature, none of the layers healed adequately. Although environment temperature had less impact on the lower layers closer to the print bed, 100% healed layer number increased when the chamber temperature increased. The model predictions were in good agreement with the experimental data, particularly for the mid-part of FFF PEEK cubes printed in both FFF machines.

Corresponding author: Cemile Basgul, MS, Implant Research Center, Drexel University, 3401 Market St, Suite 345, Philadelphia, PA 19104, USA, cb997@drexel.edu, Phone: +1 267 469 84 10.

## Graphical Abstract

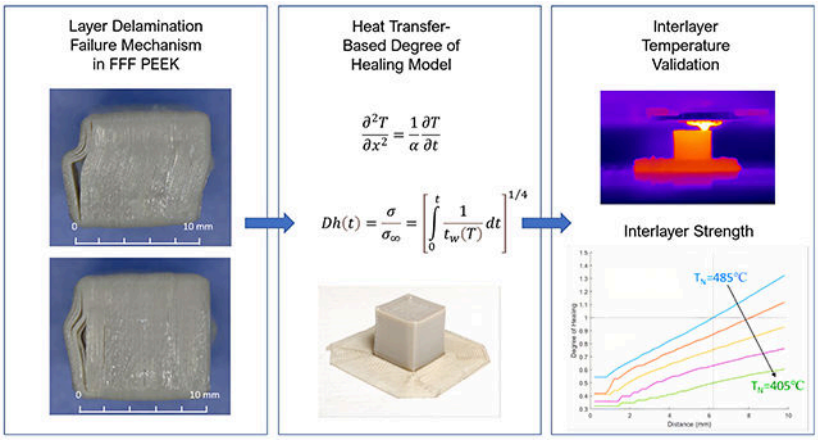


### Keywords

Fused filament fabrication; PEEK; heat transfer modeling; non-isothermal healing; medical additive manufacturing; interlayer debonding

## 1. Introduction

Fused Filament Fabrication (FFF) systems as an Additive Manufacturing (AM) method have inspired both research and industry to manufacture polyetheretherketone (PEEK) implants [1–4]. FFF has the material conservation advantage by requiring filament as the form of material over powder systems (e.g., selective laser sintering (SLS)) that have been investigated to manufacture PEEK implants [5–7]. In addition to savings over expensive medical grade PEEK material, FFF technologies are more suitable in a hospital setting compared to SLS printers, regarding contamination and sterility promoting research towards AM at point-of-care (POC) [8–10]. Although FFF PEEK implants have shown their potential [4, 11, 12], layer delamination has been indicated as the failure mechanism for FFF PEEK spinal and cranial implants so far [1, 9]. Due to the high processing temperatures of PEEK, it is crucial to avoid layer delamination by ensuring proper healing between the PEEK layers [13]. This failure mechanism is strongly associated with the thermal conditions controlled by direct and indirect thermal parameters [1, 14]. In FFF systems, extruded lines build up the layers, which are laid consecutively on top of each other until they form the final part. During these processes, heat transfer occurs between the deposited layers as well as from layers into the print bed and the print environment. These heat transfer processes determine the temperature history of the merging layers, which plays a critical role in healing between the layers, hence the unity of the part and its mechanical strength. It is essential to quantitatively address the interlayer strength of FFF PEEK for further enhancement of an FFF implant with superior mechanical properties.

Researchers have previously analyzed the thermal conditions of FFF systems for low-temperature polymers via the heat transfer model (HTM) to understand the challenges in FFF, such as warping, adhesion, and layer delamination [14–20]. However, most of

these studies focused on the temperature and adhesion of the extruded fiber (filament), which creates the layers in the build [14–16]. Thomas et al. [15] obtained the interface temperatures of filaments via analytically solving a two-dimensional (2D) heat transfer model to predict the fracture toughness of the FFF ABS parts. Similarly, a study combined a one-dimensional (1D) HTM to estimate the cooling profile and a polymer sintering model to investigate the bond formation between the filaments in FFF ABS parts [16]. Similarly, Costa et al. [14] analyzed the filament adhesion on FFF ABS parts via a 1D HTM to estimate the filament temperatures and healing. In addition to low-temperature polymer studies, filament temperature distribution was assessed with a 1D HTM to investigate the surface roughness of FFF PEEK parts [21]. Other than exploring the filament temperature history, HTM was recognized to determine the layer temperatures, in which complications such as warping and cracking in the large-scale carbon-fiber-reinforced acrylonitrile butadiene styrene (CFR-ABS) FFF were studied [18].

Moreover, some studies utilized the layer temperature distribution gathered from HTMs in a non-isothermal degree of healing (DOH) formula, defined by Yang et al. [22], to assess the filament healing in low-temperature FFF builds [14, 19]. The filament adhesion in FFF ABS parts was showed locally, where below 100% healing was indicated as poor adhesion [14]. Furthermore, Yin et al. [19] studied the filament bonding strength in low-temperature bi-material printing (thermoplastic polyurethane (TPU) and ABS). Nonetheless, a few studies which were developed for low-temperature polymer FFF validated the heat transfer models [14, 18, 20]. Costa et al. [14] compared the ABS filament temperatures obtained via the 1D HTM with the experimental filament temperatures measured via a thermal camera. Besides, Ravoori et al. [20] used a thermal camera to measure the polylactic acid (PLA) filament temperatures to investigate the temperature field on the platform bed during filament dispense. Finally, one study conducted thermal camera readings to justify the layer temperatures of large-scale CFR-ABS builds predicted with a 1D HTM [18].

Improved interlayer strength to enhance the macro mechanical properties of FFF PEEK implants is necessary by addressing the issue of interlayer delamination phenomena of FFF. Despite the layer delamination failure in FFF builds, previous models mainly focused on the filament temperature distribution and healing rather than investigating the layer adhesion. Thus, a comprehensive model is crucial to understand the thermally driven healing mechanisms for parameter optimization to improve the layer healing on FFF PEEK implants. Additionally, specific validation of FFF PEEK layer temperature predictions is critical for the proposed heat transfer model before its further applications in layer healing approximations. Hence, we asked: (1) Can a 1D heat transfer model coupled with a non-isothermal degree theory predict the interbonding strength of FFF PEEK layers? (2) Will the enhancement of key FFF process temperatures (print bed ($T_B$), chamber ($T_C$), and nozzle temperatures ($T_N$)), yield a higher degree of healing, and hence improved interlayer adhesion? (3) How is the 1D HTM affected by a different FFF system with additional heat transfer mechanisms?

# 2. Materials & Methods

## 2.1 Interlayer Strength Modeling

**2.1.1 Heat Transfer Model (HTM)—**A 1D transient heat transfer model was developed to predict the temperatures of layers and interlayers by simulating the deposition process in 3D printing PEEK parts. The initial geometry (Fig. 1 (A)) was inspired by the XZ plane of the standard cage design used in the previous studies [1]. 1D design of the model was justified by the geometric characteristics of the extruded layer: (1) Considering the 0.2 mm layer height while printing with 0.4 mm nozzle diameter, the layer dimensions will be 10x10x0.2 $mm^3$. Since the layer dimensions in the x and y directions are 50 times bigger than the z-direction, the heat transfer from a layer is considered to occur at most in the z-direction (Fig. 1). It was assumed that a uniform temperature distribution throughout the cross-section (i.e., variations in the temperature across the layer thickness are not taken into consideration).

Three main temperatures are affecting the heat transfer through layers in this model, which are, print bed temperature ($T_B$); material deposition temperature, referred to as the nozzle temperature, ($T_N$); and the environment temperature in the closed chamber where the part is printed ($T_C$). $T_N$ and $T_B$ were selected based on the FFF machine settings that were used to print FFF PEEK cages in the previous studies [1] and a presumptive value is selected for $T_C$ (Table 1). These temperatures were considered to be constant through the print. A layer was examined as a rectangle bar stacked on top of each other at certain time intervals ($t$), which is indicated as layer deposition time in the model. The layer deposition time was calculated experimentally which was the time spent to print a layer of the initial cube geometry at 2000 mm/min.

Initial conditions (IC) were as follows: For a single layer, the initial temperature upon deposition was assumed uniform and equal to the nozzle temperature ($T_N$). The temperature at the bottom surface of the specimen was set to be equal to the temperature of the building stage ($T_B$), while for other surfaces exposed to air, the convection boundary conditions were applied. The boundary conditions (BC) of a layer were defined specifically and updated for all layers after each layer deposition to simulate the 3D printing process. The derivation of the convection coefficient (h), applied in convection BC equations, was based on the previous calculations in the literature (Eq. 1 & Table 2) [18].

$$h = \frac{Nu_L k_f}{L} \tag{1}$$

The unsteady-state heat conduction equation in a one-dimensional rectangular coordinate system to obtain the temperature distribution for constant thermophysical properties was utilized and solved via finite difference approximation with an explicit method [25]. If the temperatures are known at locations $n-1$, $n$, and $n+1$ at a certain time '$p$', the temperatures after a time increment ($\Delta t$)($T_n^{p+1}$) can be calculated by the equation with variables indicated in Table 1:

$$T_n^{p+1} = \left[1 - \frac{2\alpha\Delta t}{(\Delta x)^2}\right] T_n^p + \frac{\alpha\Delta t}{(\Delta x)^2}(T_{n+1}^p + T_{n-1}^p) \quad (2)$$

The above Eq. 2 is applicable to the present conduction boundary conditions and the internal grid points. If there is convection on the boundary, the temperatures at the boundary node were calculated via 'Equation 3' defined by the energy balance equations [25]. Similarly, if the temperatures are known at locations $m-1$, $m$, and surface '$\infty$' at a certain time '$p$', the temperatures after a time increment $(\Delta t)(T_m^{p+1})$ can be calculated by the equation with variables indicated in Table 1:

$$T_m^{p+1} = \frac{\alpha\Delta t}{(\Delta x)^2}\left\{\left[\frac{(\Delta x)^2}{\alpha\Delta t} - 2\frac{h\Delta x}{k} - 2\right] T_m^p + 2T_{m-1}^p + 2\frac{h\Delta x}{k}T_\infty\right\} \quad (3)$$

Eqs. 2 and 3 were used to calculate the temperatures at the nodes depending on the boundary conditions at each time step. Additionally, the stability of Eq. 2 and Eq. 3 was ensured with the below conditions, which defined the time step ($\Delta t$) for model calculations.

$$\frac{\alpha\Delta t}{(\Delta x)^2} \leq 0.5 \quad (4)$$

$$\frac{(\Delta x)^2}{\alpha\Delta t} \geq 2\left(\frac{h\Delta x}{k} + 1\right) \quad (5)$$

Custom scripts were developed using MATLAB 2018b to calculate the heat transfer coefficient and solve the heat transfer model. The layer temperature histories obtained from the heat transfer model were then implemented to an interface healing model to calculate the degree of layer healing.

**2.1.2 Degree of Healing Model—**The temperature history of interlayers calculated via the HTM was used to determine the degree of healing between two layers of PEEK parts produced via FFF (Fig. 2). In the literature, it is stated that the healing mechanisms are active only when the material temperature is above the melting point for the semicrystalline polymers, like PEEK [22]. Thus, to calculate the degree of healing for each interlayer point (n=49), temperature distributions between the deposition temperature (485°C) and the melting temperature of PEEK (343°C) were extracted from the HTM of PEEK.

The non-isothermal degree of healing ($Dh(t)$) as a function of time utilized in this study was defined as the ratio of the instantaneous bond strength ($\sigma$) to the ultimate bond strength ($\sigma_\infty$) by Yang and Pitchumani, where $t_w$ is temperature-dependent welding time and the temperature is changing with time. [26].

$$Dh(t) = \frac{\sigma}{\sigma_\infty} = \left[\int_0^t \frac{1}{t_w(T)} dt\right]^{1/4} \quad (6)$$

In this study, the welding function formula previously calculated for PEEK by Lee and Springer is used, where $T$ is the time-dependent temperature function [27].

$$t_w = \left(\frac{1}{44.1} exp \frac{3810}{T}\right)^4 \quad (7)$$

Interlayer degree of healing values were calculated for the FFF PEEK to construct under the conditions that were previously studied for FFF PEEK cages. Additionally, three main temperatures in the FFF system ($T_B$, $T_N$, $T_C$,) were varied to evaluate their effects on the healing of FFF PEEK layers. Five different values with 20°C increments (from 130°C to 210°C), 20°C decrements (from 485 to 405°C), and 40°C increments (from 80 to 240°C) for the print bed, nozzle, and chamber temperatures, respectively, were investigated while all other parameters, except time step and convection coefficient, were kept constant. Custom scripts developed for DOH were implemented into the HTM model in MATLAB 2018b.

## 2.2 Measurement of Layer Temperatures

**2.2.1 Experimental Setup for Temperature Measurements—**To validate the layer temperatures obtained by the HTM, the initial cube design (10x10x10 $mm^3$) was printed with industrial-grade PEEK filament (Apium PEEK 4000) both in 2nd (P220) and 3rd generation (M220) FFF machines (Apium Additive Technologies GmbH, Karlsruhe, Germany) (Supplementary Fig. 1).

The filaments used in this study were dried at 120°C for four hours prior to printing. In the P220 machine, which was introduced as the industrial 3D printer for high-performance materials, heating elements are the extruder, glass print bed, and the metal heated plate (referred to as the zone heater) around the extruder (nozzle) (maximum temperatures of 540°C, 160°C, and 250°C, respectively). On the other hand, M220 is the first 3D printer that is invented for medical PEEK products and implants by ensuring a sterile print environment. Thus, the prints are deposited on a specifically designed metal print bed, which allows filtered hot airflow in a particle-free circuit (maximum temperature of 280°C). The STL file of the cube was created using commercially available software (SolidWorks 2016). Simplify 3D software (available commercially) was used to construct the g-codes from the STL file for both FFF machines. To increase the adhesion between the cube and the print bed in the P220 machine, in addition to the brim (Fig. 3 (B–D)), one layer of Dimafix® (DIMA 3D Printers) solution was applied onto the heated bed prior to printing. For the M220 machine, the slicing software of Apium embedded in the printer creates an automated raft for every part (Fig. 3 (E)). To avoid contamination, the combination of the raft and print bed design in this machine extinguishes the requirement for any additional adhesives.

FFF PEEK cubes were printed under 2000 mm/min print speed with a 0.4 mm nozzle diameter and 0.2 mm layer thickness in both machines (as studied in the HTM) (Table 3). Temperature settings were constant in both printers for the temperature validation of the layers with the HTM.

When printing the PEEK cubes with defined settings in both FFF printers, thermal videos were recorded at 50 Hz (frames per second) with a FLIR A655sc machine (FLIR, Wilsonville, OR). The accuracy of the camera was ±2°C that is established by yearly calibrations from the manufacturer. As suggested by the manufacturer, the camera was positioned approximately 25 cm away from the heat source (the print area). Since the temperature readings were affected by an object placed between the print build and the camera (i.e., the 3D printer door), an insulation board in both machines surrounded the IR camera to preserve the heat while the printer door remained open (Supplementary Fig. 1).

**2.2.2 Image Analysis—**Thermal videos collected with a FLIR A655sc camera were converted into the TIFF image stacks which contain the temperature information via ResearchIR software (FLIR, Wilsonville, OR) for further analysis in MATLAB 2018b. Second, the region of interests (ROI) was defined conforming to the object location, and the image stacks were cropped accordingly to 150 by 150-pixel frames (Fig. 4).

In addition, the “Sobel Edge Detection Algorithm” [28] was conducted to detect the edges defined near the printed cubes for both machines. According to the movement of these edges during the FFF processes, the beginning and end frames, in between where the cubes were being printed, were determined for the layer temperature history. After defining the beginning and end frames where the part is being printed, the mid-pixel of the object was selected to analyze the temperatures in both printers. Due to the set-up limitations of the IR camera, pixel number through the printed cube was interpolated to acquire an exact equivalent of the pixel numbers and the layer numbers (n=50).

In addition, key FFF temperatures ($T_N$, $T_B$, and $T_C$) utilized in the model were calculated experimentally for model validation in both printers. For the material deposition temperature (referred to as the nozzle temperature), the maximum temperatures from each layer (n=50) were averaged in MATLAB 2018b. For the bed and environment temperatures, the mean value was calculated from five different regions selected in the thermal videos with the help of ImageJ (U. S. National Institutes of Health, MD, USA). Custom scripts using MATLAB 2018b were developed to fulfill previously described steps for layer temperature history of FFF PEEK cubes printed with 2$^{nd}$ (P220) and 3$^{rd}$ (M220) generation machines.

## 3. Results

### 3.1 Heat Transfer based Degree of Healing Model

Both interlayer (n=49) and layer (n=50) temperature distributions were obtained for a 10 mm high 3D printed PEEK construct with 50 layers via HTM. It was observed that both layer and interlayer temperatures were decreasing faster when they were closer to the print bed (130°C). The temperatures were staying higher for the layers which were closer to the top of the object, where the convection boundary condition was effective (Fig. 5). In

addition, the reheating effect of consecutive layers is readily simulated. Depending on the layer and/or interlayer, the first consecutive layer's effect was the biggest and it gradually decreased. Finally, after ten layers that effect was almost invisible.

In addition, it was observed that the degree of healing across the 10 mm FFF PEEK build increased linearly from lower to upper layers in reference to the print bed, where DOH>1 indicates fully healed interfaces (Fig. 6). The predicted degree of healing was between 0.54 and 1.32 for interlayers with an average of 0.91 under initial temperature settings (Table 4). The degree of healing was lower than 1 for the first 30 interlayers, which meant that these layers were cooling down faster before 100% strength was achieved. Thus, to reach 100% healing for these interlayers, theoretically, more time is needed between the designated temperatures.

Three main temperature effects on the degree of healing were shown via the heat transfer-based degree of healing model (Fig. 6, Table 4). For the bed temperature ($T_B$), the degree of healing was calculated for five different temperatures with 20°C increments (130, 150, 170, 190, and 210°C) (Fig. 6(A)). Increasing the temperature of conduction boundary condition from 130 to 210°C, referred to as print bed, increased the minimum, average and maximum healing (22%, 11%, and 21%, respectively). From minimum to maximum bed temperatures (80°C difference) investigated in the model fully healed layer number was increased from 19 to 29 (53%).

Since the initial nozzle temperature (485°C) was already close to the decomposition temperature of PEEK [29], the effect of nozzle temperature on the interlayer degree of healing was studied via temperature decrements (485, 465, 445, 425, and 405°C) (Fig. 6 (B), Table 4). Decreasing the nozzle temperature from 485 to 405°C decreased the minimum, average and maximum healing (41%, 51%, and 54%, respectively). With a 20°C decrease in the nozzle temperature (from 485 to 465°C), the unhealed interlayer number increased to 40 interlayer points (33%). 445°C and below nozzle temperature, none of the interlayers were 100% healed (n=49) with average layer healing between 45-68%. Finally, five different chamber (internal) temperatures ($T_C$) were investigated with 40°C increments (80, 120, 160, 200, and 240°C) (Fig. 6 (C), Table 4). Increasing the chamber temperature from 80 to 240°C increased the average and maximum healing (18% and 11%, respectively), whereas did not change the minimum healing. Additionally, the 100% healed layer number increased to 27 layers (42%) with the highest chamber temperature.

### 3.2 Heat Transfer Model Validation

Model parameters were revised in the HTM with the experimental temperature implementation for both printers' layer temperature validations. Additionally, since the raft, printed automatically underneath the FFF cube for the M220 machine, changed the length of the part in the HTM, the number of layers, and nodes were modified accordingly for further validation (Table 5).

As mentioned in the model, the temperatures stayed higher for longer periods from the bottom to the top of the FFF PEEK cube when printed in the P220 machine (Fig. 7). The temperature decrement observed while cooling was steeper for the upper layers. When the

layer temperature distributions from the HTM and the experimental data recorded from the P220 machine were compared, it was recognized that the model assumptions were closer to the experimental data for the mid-layers of the cube. The model approximated the lower layer temperatures colder compared to the experimental temperatures. However, the difference between the model and experimental layer temperature history was diminishing when approaching the upper layers through the FFF PEEK build. Moreover, the model predictions for the top layers stayed slightly higher than the experimental temperatures. For instance, 1st layer's temperature dropped from 333°C to 195°C approximately in the first two minutes and slowly decreased to 156°C by the end of the print. Whereas the maximum temperature observed for the 11th layer was 343°C which decreased to 217°C in two minutes and was 173°C at the print end. The maximum layer temperature, the temperature at two minutes and before cooling started were 344°C, 229°C, and 193°C, respectively for the 21st layer. The maximum temperature started at 346°C and then reduced to 235°C after 120 seconds for the 31st layer. The temperature measured before cooling started was 217°C. Finally, for the last layer selected (41st layer), the highest layer temperature was 347°C. After two minutes, the layer was already in the cooling stage and the temperature was 217°C. Before cooling started, the last temperature measured was 241°C.

Similarly, for M220 prints, the model predicted the layer temperature distributions lower for the lower layers and overlapped well for the mid-part of the object (Fig. 8). By the 30th layer, the model approximations started to remain higher for layers and the difference increased slightly to the top of the FFF PEEK cube. Additionally, after the first quarter of the cube, the cooling profile of the HTM was recognized to remain higher than the experimental readings. For instance, the first layer's temperature (327°C) decreased to 220°C in the first two minutes and reached 185°C by the end of the print (Fig. 8 (A)). For the 11th layer, the highest temperature was 316°C that decreased to 226°C in two minutes and 190°C when the cube was completely printed (Fig. 8 (B)). The highest layer temperature, the temperature at two minutes, and the temperature at the end of the FFF process were 317°C, 228°C, and 199°C, respectively for the 21st layer (Fig. 8 (C)). The temperature readings of the 31st layer were 318°C, 227°C, and 211°C for the highest layer temperature, the temperature at two minutes, and the temperature at the end of the FFF process, respectively (Fig. 8 (D)). For the 41st layer, the temperature decreased from 318°C to 214°C in two minutes and print ended for the layer before two minutes where the temperature was 224°C (Fig. 8 (E)).

Other than the model validation of the layer temperatures during printing and cooling processes, the model predictions of layer temperatures at the very beginning of the print (first minute) were investigated which are crucial for healing mechanisms (Fig. 9). Despite the experimental data when plotted for shorter times appearing to be noisier, it was acknowledged that the HTM layer temperatures agreed accurately with the FFF layer temperatures in both machines, specifically after the first 20 layers.

## 4. Discussion

Interlayer delamination has been identified in FFF PEEK implants as a concern due to its association with mechanical strength [13]. As heat management plays a key role in determining the bonding strength of layers to achieve stronger FFF parts, investigating

the layer adhesion with a heat transfer-based polymer healing model is a valuable step in assessing their mechanical strength. In this study, a 1D transient heat transfer-based, non-isothermal polymer healing model was developed to predict the interlayer strength for a FFF PEEK build. The specific sections from interlayer temperature distributions obtained via HTM in which healing occurs were implemented into the healing model to predict the strength percentage across the FFF PEEK build. Additionally, to validate the heat transfer component of the model, experimental layer temperatures were measured while printing the FFF PEEK cubes in industrial ($2^{nd}$) and medical ($3^{rd}$) generation FFF machines. The model showed that healing between the layers increases linearly from the bottom, where the part is in contact with the print bed, to the top of the part. Under the settings used to print spinal implants [1], more than half of the layers need to spend more time above critical temperature to reach 100% interlayer strength. Absolutely healed layer number could be increased by raising the main temperature settings, however, printability under these settings should be experimentally evaluated. As the HTM model presented, experimental layer temperatures also stayed higher for upper layers compared to the lower layers of the FFF PEEK cube for both printers. For both the $2^{nd}$ (P220) and $3^{rd}$ (M220) generation machines, the best agreement between the model predictions and experimental data for the printing period was in the mid-part of the FFF PEEK build, in which the cooling profile remained slightly higher. Additionally, short-term approximations (the first minute of the print) for both machines, which would be necessary for the degree of healing studies, were more consistent after the $20^{th}$ layers. The model presented here helps to determine the layers on the FFF PEEK builds printed with defined parameters that are not healed properly, which could induce layer delamination under loading conditions due to insufficient healing. The results of this study support that the heat transfer-based non-isothermal polymer healing model is a suitable tool to investigate both the direct and indirect thermal parameters in a FFF system and quantify the interlayer strength of FFF PEEK parts.

It was demonstrated via the HTM that temperatures from the upper layers remain higher for a more extended period because their base (aka conduction boundary) was influenced by the previously extruded layers. The more layers below a newly deposited layer, the higher boundary temperature which preserves the heat of the deposited layer was prolonged. It is also essential to recognize the reheating effect of the continuous layers. The first ten consecutive layers were decreasingly raising the temperature of the initial layer. This reheating phenomenon is also presented by previous models for low-temperature FFF [17–19]. However, due to the closer gap between the bed and extrusion temperatures while printing low-temperature polymers, the reheating effect was less evident and critical in layer healing compared to FFF of PEEK. Reheating the interlayer above PEEK's melting temperature might supplement healing, which is beyond the scope of this work and needs further investigation. According to the model, we found an association between the significant temperatures ($T_B$, $T_N$, and $T_C$) and the interlayer strength in a FFF PEEK build. Zhang et al. [17] also stated that these three temperature settings are primary factors determining the temperature variation in FFF PLA parts. This is primarily driven by the welding process, for which the layers should remain above the critical temperature enough to ensure adequate healing. Increasing these temperatures is increasing the time spent between the extrusion temperature and the melting temperature of PEEK layers. The most

significant difference in 100% healed layer number was ensured with the nozzle temperature adjustment. Decreasing the nozzle temperature by 20°C to 465°C almost halves totally healed layers (47% less) and below 445°C ($T_N$) none of the layers could achieve 100% healing. Similarly, Coasey et al. [30] showed that the degree of filament healing increased more than two times with the same amount of increase (20°C) in the nozzle temperature for a FFF ABS interface point. They mentioned the extrusion temperature's dominant effect on the degree of healing due to its direct relation to the reptation time. In the same manner, Ko et al. [31] expressed the dramatic increase in interface strength of filaments by increasing the printing temperature for PC-ABS. In addition to low-temperature polymer FFF studies, Wang et al. [21] investigated the flow parameters including the nozzle temperature for FFF PEEK to optimize the surface roughness. They recommended using higher heating temperatures above 440°C to improve density, reduce internal effects and surface roughness, and strengthen the adhesion between the printed layers and filaments in FFF PEEK builds. Furthermore, the second dominant temperature setting in layer healing for FFF PEEK was the print bed temperature ($T_B$). Increasing $T_B$ not only increased the minimum, maximum, and average degree of healing over the FFF PEEK part but also increased the totally healed layer number by 53% ($T_B$ from 80°C to 210°C). Previously, Yin et al. [19] increased the build plate temperature (from 30°C to 68°C) for ABS-TPU and claimed that the role of the building stage is more obvious than two conditions ($T_N$ and $T_C$). Finally, regarding the tested conditions in this model, the chamber temperature was found to be the least dominant temperature in the degree of interlayer healing. Across the chamber temperatures tested in the model (80-240°C), the minimum degree of healing was not affected signifying that environment temperature has less impact on the lower layers of the FFF PEEK part. Yet, 42% increment in perfectly healed layers was managed with a 160°C increase in chamber temperature. Although theoretical calculations suggest the enhancement in layer healing via main temperature increments, this should be experimentally tested since efficient cooling of layers is critical which allows sequential layer accumulation to achieve a successfully 3D printed part.

Moreover, as revealed by the HTM, experimental layer temperatures in both machines were higher for the upper layers compared to the lower layers in reference to the print bed. The higher temperatures for the longer were declared for the upper filaments compared to the lower filaments which were in physical contact with the print bed for FFF ABS as well [14]. The model estimations were lower compared to the experimental temperatures for the layers closer to the print bed. This might be due to the actual bed temperature in the print area being higher than the value utilized in the model. Additionally, the sandwich effect of the plate around the nozzle and the print bed might be accelerating the bed temperature which would be more remarkable for lower layers. A similar gap between the first layer temperature predictions and the experimental temperatures was recognized previously for a 3D printed thin CFR-ABS wall via thermal readings [18]. The gap between the model and experiments diminished as mid-layers were approached, since the layer below, for which the most accurate temperature approximation was done in the model according to the maximum layer temperatures measured via thermal videos, was the new boundary. Thus, the model predictions for FFF PEEK layers printed in both medical and industrial FFF printers were in good agreement after the $20^{th}$ layers, which was more recognizable when the convergence

was investigated in the first minute of the print. The reason why the convergence happened earlier for the medical FFF machine was the automated raft involved in the model as well as in the experiments. This confirmed our interpretations about the dominance of the conduction boundary temperature in the model, suggesting the print bed and its variation during the FFF process need to be investigated further in detail when adopting this model. Finally, as the printing profile approximations of the model converged to the experimental temperatures, the cooling profile of the model was slightly higher especially for the medical FFF printer due to the additional convection effect.

There were some limitations involved in this study. For the first part of the model, considering the layer dimensions (10x10x0.2 $mm^3$), the heat transfer of the FFF part was modeled as 1D. This assumption was supported by the idea that most heat transfer will happen in the layer thickness direction. For the second part of the model in which healing was calculated, the welding function was based on an equation developed experimentally in the literature for injection-molded PEEK [22]. Moreover, the temperature distribution between the melting and the deposition temperatures was assumed to be linear for simplicity in the degree of healing calculations, which could be investigated in detail in the future. In addition, material-dependent values accessed from the literature represent the bulk PEEK properties. These material dependents and thermal parameters were considered to be constant during 3D printing for the model. More investigation is suggested under unstable FFF process conditions in addition to the different manufacturing settings. For experiments, the thermal measurements were collected leaving the printer door open in both machines due to the capability of the thermal camera. However, to preserve the heat inside the printers as much as possible, insulation boards were covered around the camera during recordings. Further studies should consider the infrared signal reflection from the insulation board to the printing environment. Additionally, the FLIR camera was required to be placed at a certain distance (25 cm) from the heat source (the print area) for safety, which limited the resolution of the thermal videos/images. Finally, although the previously developed HTM with a constant conduction boundary at the print base was applied for the medical (M220) printer, there was additional convective heat transfer occurring due to the hot air flow underneath the print bed which requires additional considerations in the future.

Fundamentals of FFF require detecting the optimum spot where the layer temperatures should be low enough to allow further layer build, but in the meantime high enough to accomplish the maximum healing and strength between the layers for a solid part. To produce mechanically stable FFF PEEK implants for AM-POC, it is vital to understand the heat transfer and layer healing mechanisms of FFF. The model presented here proves a theoretical method to evaluate both thermal and non-thermal parameters in FFF that could be used for FFF implants to reduce the time-consuming experimental steps in the future. Initial investigations for model validation were presented in FFF PEEK layers printed with industrial and medical generation FFF machines. The correlation between the model and the experimental results from different FFF systems supports the promising future of the proposed model for FFF PEEK implants. The associations observed between the manufacturing temperatures and the layer healing highlight the potential of the model in parameter optimization for different designs of FFF PEEK implants.

## 5. Conclusions

This study investigated a 1D heat transfer-based non-isothermal degree of healing model to determine the interlayer strength of PEEK layers when 3D printed. The model helped to define the insufficiently healed layers through FFF PEEK build, which could trigger layer debonding under biomechanical loads for FFF PEEK implants. According to the model, the degree of healing increased linearly from lower, closer to the print bed, to the upper layers of the FFF PEEK cuboids. With the FFF settings conducted to print cages, more than half of the layers were not healed completely, which can be enhanced via increasing the key FFF temperatures (nozzle, bed, and environment) based on the model. Experiments from both printers confirmed that the upper FFF PEEK layers, in reference to the build plate, stayed higher compared to the lower layers. In both machines, the model predictions converged the experimental layer temperatures around mid-layers. For the medical generation printer, the convergence happened earlier due to the additional raft layers underneath the part. Since approximated layer temperatures were depended on maximum layer temperatures measured via thermal videos, the newly deposited layer as conduction boundary was the most accurate boundary temperature. The dominance of the conduction boundary (print bed) especially for the lower layers was recognized.

## Supplementary Material

Refer to Web version on PubMed Central for supplementary material.

## Acknowledgements

This study was supported by NIH-R01 AR069119 and ThinkSwiss Research Scholarship 2020. We would also like to thank Apium for their collaboration, helpful advice, and fruitful discussions, and the University of Basel, Department of Biomedical Engineering for the FLIR machine used in the experiments.

## Glossary

| | |
|---|---|
| **FFF** | Fused Filament Fabrication |
| **AM** | Additive Manufacturing |
| **PEEK** | Polyetheretherketone |
| **1D** | One-dimensional |
| **HTM** | Heat transfer model |

## References

[1]. Basgul C, MacDonald DW, Siskey R, Kurtz SM, Thermal localization improves the interlayer adhesion and structural integrity of 3D printed PEEK lumbar spinal cages, Materialia 10 (2020) 100650. [PubMed: 32318685]

[2]. Delaney LJ, MacDonald D, Leung J, Fitzgerald K, Sevit AM, Eisenbrey JR, Patel N, Forsberg F, Kepler CK, Fang T, Kurtz SM, Hickok NJ, Ultrasound-triggered antibiotic release from PEEK clips to prevent spinal fusion infection: Initial evaluations, Acta biomaterialia 93 (2019) 12–24. [PubMed: 30826477]

[3]. Prechtel A, Stawarczyk B, Hickel R, Edelhoff D, Reymus M, Fracture load of 3D printed PEEK inlays compared with milled ones, direct resin composite fillings, and sound teeth, Clinical Oral Investigations (2020).

[4]. Zhang C, Wang L, Kang J, Fuentes OM, Li D, Bionic design and verification of 3D printed PEEK costal cartilage prosthesis, Journal of the Mechanical Behavior of Biomedical Materials 103 (2020) 103561. [PubMed: 32090953]

[5]. Berretta S, Evans K, Ghita O, Additive manufacture of PEEK cranial implants: Manufacturing considerations versus accuracy and mechanical performance, Materials & Design 139 (2018) 141–152.

[6]. Zhong R, Xie Z, Liao Y, Li Y, Huang C, Clinical application of triangular parabolic PEEK mesh with hole button produced by combining CAD, FEM and 3DP into cranioplasty, Biomedical Research 29 (2018).

[7]. El Halabi F, Rodriguez JF, Rebolledo L, Hurtos E, Doblare M, Mechanical characterization and numerical simulation of polyether-ether-ketone (PEEK) cranial implants, J Mech Behav Biomed Mater 4(8) (2011) 1819–32. [PubMed: 22098881]

[8]. Honigmann P, Sharma N, Okolo B, Popp U, Msallem B, Thieringer F, Patient-Specific Surgical Implants Made of 3D Printed PEEK: Material, Technology, and Scope of Surgical Application, 2018.

[9]. Sharma N, Aghlmandi S, Cao S, Kunz C, Honigmann P, Thieringer FM, Quality Characteristics and Clinical Relevance of In-House 3D-Printed Customized Polyetheretherketone (PEEK) Implants for Craniofacial Reconstruction, Journal of clinical medicine 9(9) (2020).

[10]. Honigmann P, Sharma N, Schumacher R, Rueegg J, Haefeli M, Thieringer F, In-Hospital 3D Printed Scaphoid Prosthesis Using Medical-Grade Polyetheretherketone (PEEK) Biomaterial, BioMed Research International 2021 (2021) 1301028. [PubMed: 33506009]

[11]. Wang L, Huang L, Li X, Zhong D, Li D, Cao T, Yang S, Yan X, Zhao J, He J, Cao Y, Wang L, Three-Dimensional Printing PEEK Implant: A Novel Choice for the Reconstruction of Chest Wall Defect, The Annals of Thoracic Surgery 107(3) (2019) 921–928. [PubMed: 30403979]

[12]. Kang J, Wang L, Yang C, Wang L, Yi C, He J, Li D, Custom design and biomechanical analysis of 3D-printed PEEK rib prostheses, Biomechanics and Modeling in Mechanobiology 17(4) (2018) 1083–1092. [PubMed: 29730771]

[13]. Basgul C, Yu T, MacDonald DW, Siskey R, Marcolongo M, Kurtz SM, Structure-property relationships for 3D printed PEEK intervertebral lumbar cages produced using fused filament fabrication, J Mater Res 33(14) (2018) 2040–2051. [PubMed: 30555210]

[14]. Costa SF, Duarte FM, Covas JA, Estimation of filament temperature and adhesion development in fused deposition techniques, Journal of Materials Processing Technology 245 (2017) 167–179.

[15]. Thomas J, Rodriguez J, Modeling the fracture strength between fused-deposition extruded roads, Proc. Solid Freeform Fabr. Symp (2000) 16–23.

[16]. Bellehumeur C, Li L, Sun Q, Gu P, Modeling of Bond Formation Between Polymer Filaments in the Fused Deposition Modeling Process, Journal of Manufacturing Processes 6(2) (2004) 170–178.

[17]. Zhang J, Wang XZ, Yu WW, Deng YH, Numerical investigation of the influence of process conditions on the temperature variation in fused deposition modeling, Materials & Design 130 (2017) 59–68.

[18]. Compton BG, Post BK, Duty CE, Love L, Kunc V, Thermal analysis of additive manufacturing of large-scale thermoplastic polymer composites, Additive Manufacturing 17 (2017) 77–86.

[19]. Yin J, Lu C, Fu J, Huang Y, Zheng Y, Interfacial bonding during multi-material fused deposition modeling (FDM) process due to inter-molecular diffusion, Materials & Design 150 (2018) 104–112.

[20]. Ravoori D, Lowery C, Prajapati H, Jain A, Experimental and theoretical investigation of heat transfer in platform bed during polymer extrusion based additive manufacturing, Polymer Testing 73 (2019) 439–446.

[21]. Wang P, Zou B, Ding S, Modeling of surface roughness based on heat transfer considering diffusion among deposition filaments for FDM 3D printing heat-resistant resin, Applied Thermal Engineering 161 (2019) 114064.

[22]. Yang F, Pitchumani R, Healing of Thermoplastic Polymers at an Interface under Nonisothermal Conditions, Macromolecules 35(8) (2002) 3213–3224.

[23]. Victrex™ PEEK 450G™, 2019.

[24]. Cheng SZD, Wunderlich B, Heat capacities and entropies of liquid, high-melting-point polymers containing phenylene groups (PEEK, PC, and PET), Journal of Polymer Science Part B: Polymer Physics 24(8) (1986) 1755–1765.

[25]. Yener YK, S., Heat Conduction, CRC Press 2008.

[26]. Yang F, Pitchumani R, Nonisothermal healing and interlaminar bond strength evolution during thermoplastic matrix composites processing, Polymer Composites 24(2) (2003) 263–278.

[27]. Lee WI, Springer GS, A Model of the Manufacturing Process of Thermoplastic Matrix Composites, Journal of Composite Materials 21(11) (1987) 1017–1055.

[28]. Jiang XJ, Scott PJ, Chapter 11 - Characterization of free-form structured surfaces, in: Jiang XJ, Scott PJ (Eds.), Advanced Metrology, Academic Press 2020, pp. 281–317.

[29]. Patel P, Hull R, McCabe R, Flath D, Grasmeder J, Percy M, Mechanism of thermal decomposition of poly(ether ether ketone) (PEEK) from a review of decomposition studies, Polymer Degradation and Stability - POLYM DEGRAD STABIL 95 (2010) 709–718.

[30]. Coasey K, Hart KR, Wetzel E, Edwards D, Mackay ME, Nonisothermal welding in fused filament fabrication, Additive Manufacturing 33 (2020) 101140.

[31]. Ko YS, Herrmann D, Tolar O, Elspass WJ, Brändli C, Improving the filament weld-strength of fused filament fabrication products through improved interdiffusion, Additive Manufacturing 29 (2019) 100815.

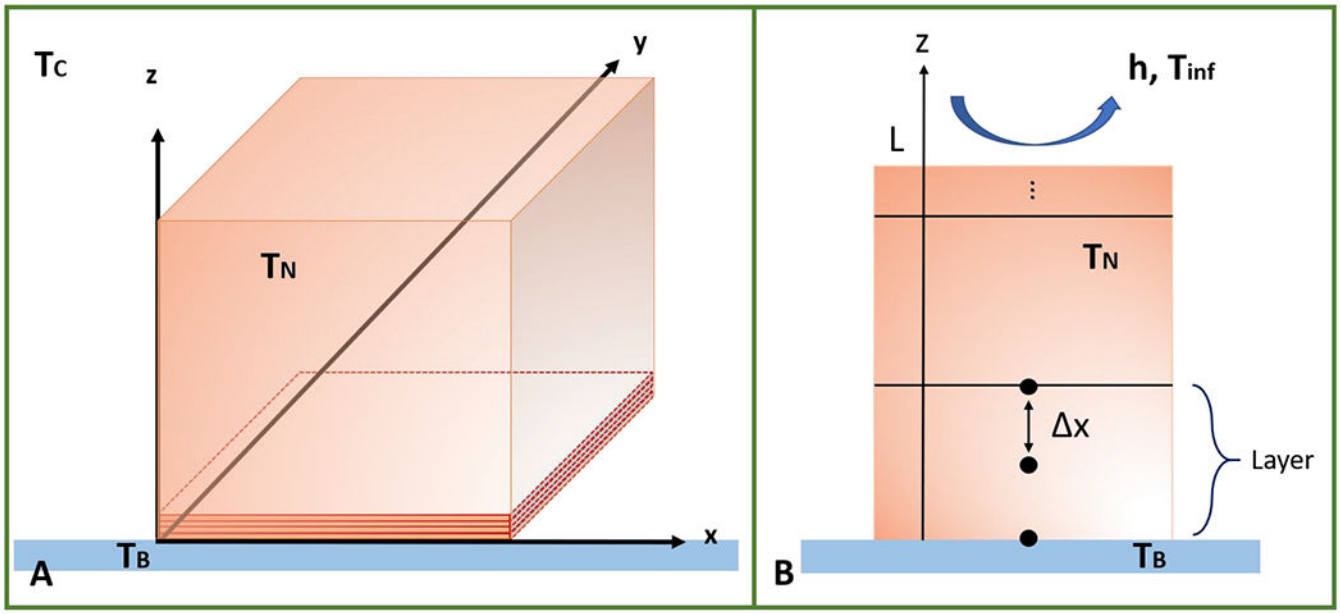


**Figure 1.**

In the physical FFF PEEK process, layers in nozzle temperature ($T_N$) are deposited on top of each other onto a print bed ($T_B$) inside a chamber ($T_C$=$T_{inf}$) (A). In the 1D HTM, a layer will have either the print bed ($T_B$) or another layer underneath as the conduction boundary and on top, the chamber temperature with a constant convection coefficient (h) will be effective as the convection boundary until a new layer is deposited (B).

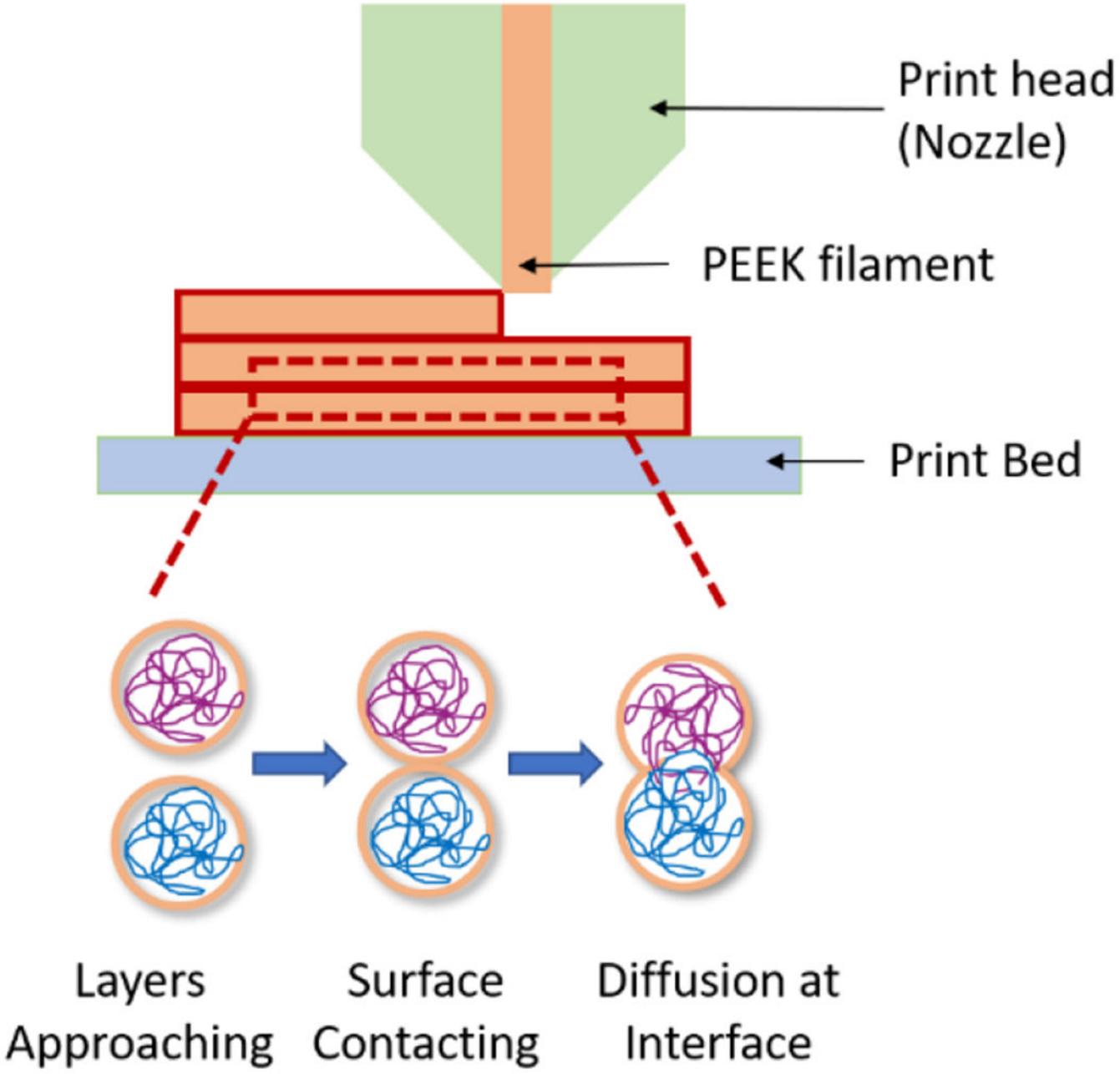


**Figure 2.**

While PEEK layers are consecutively deposited during the FFF process, healing between two layers starts with the interdiffusion across interfacial areas in contact that affects the development of interlayer adhesion strength.

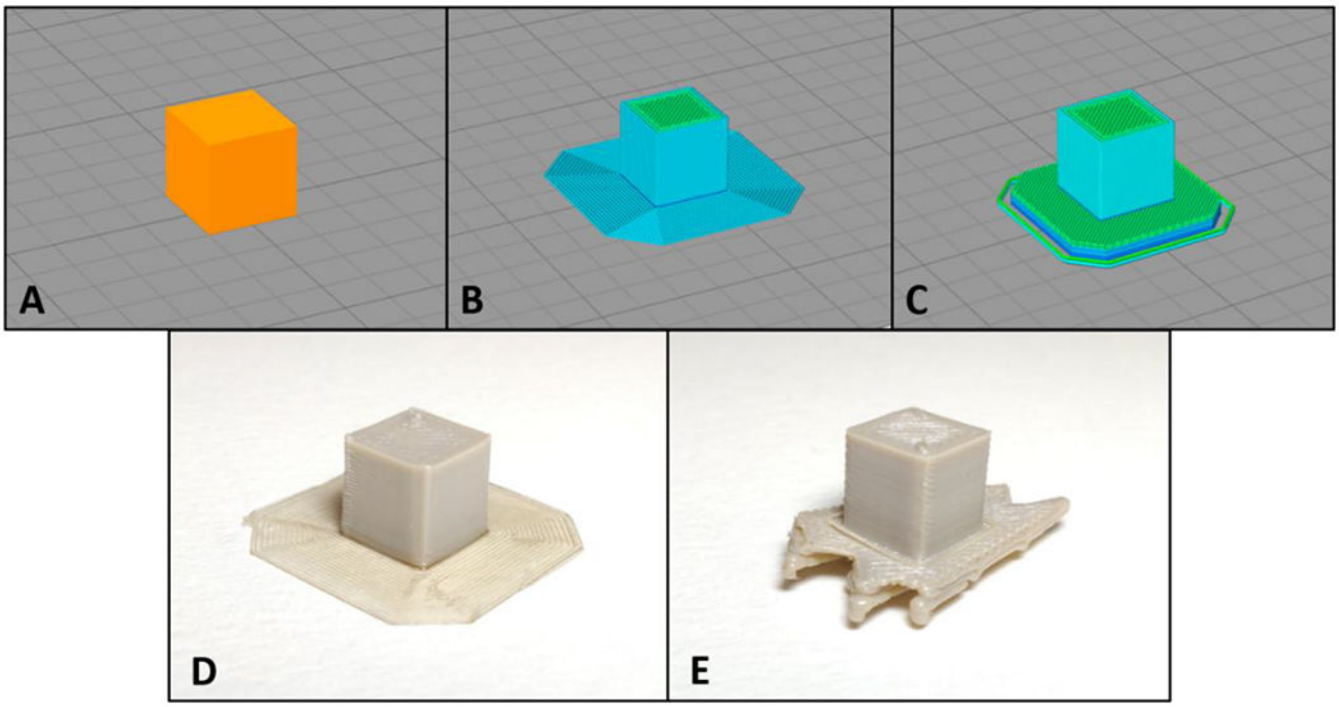


**Figure 3.**
The cube design (A), used in the HTM, was printed with the addition of brim (B-D) or raft (C-E) depending on the FFF system requirements.

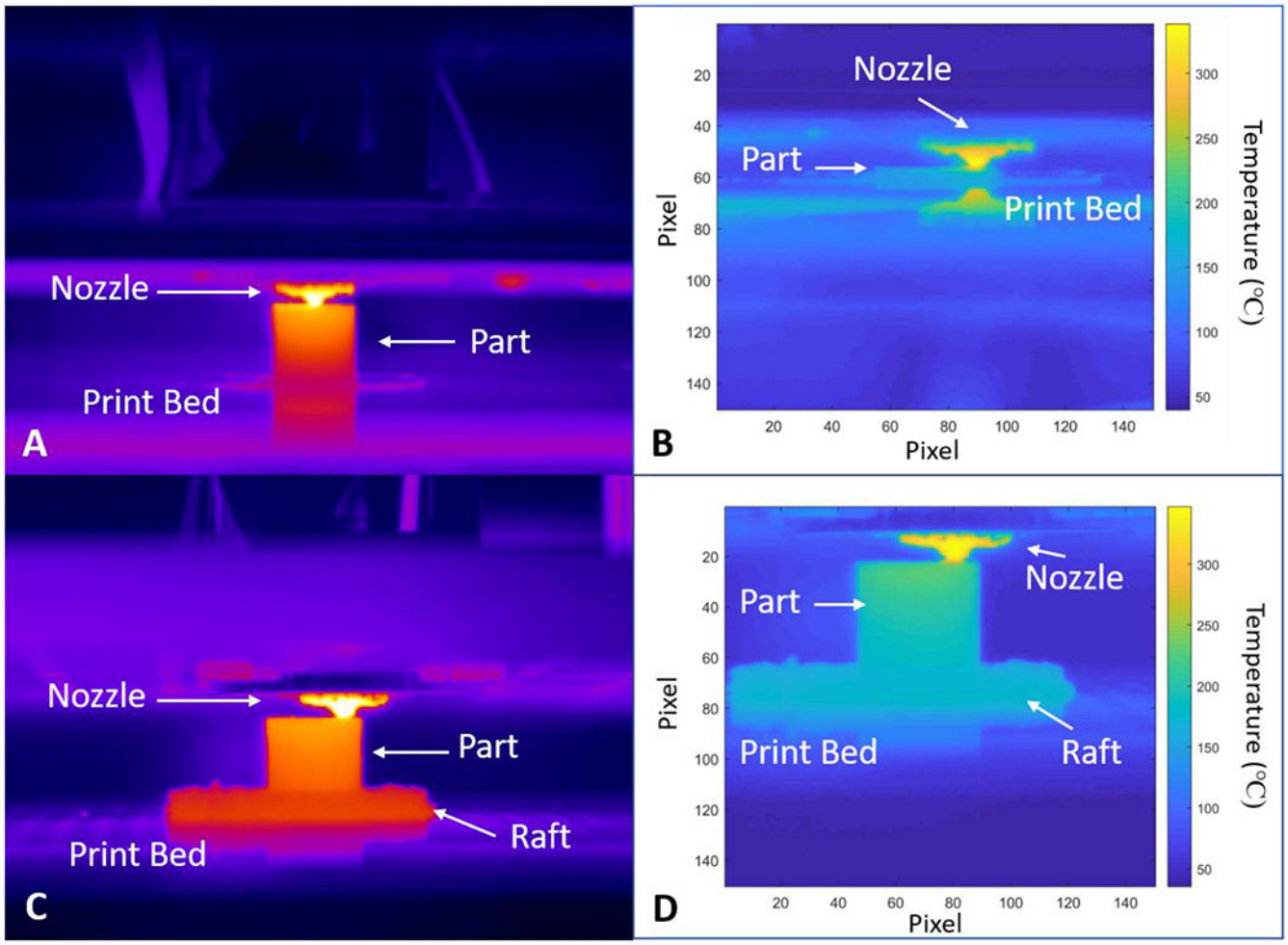


**Figure 4.**

To further analyze the thermal readings from both P220 (A-B) and M220 (C-D) machines, first, the videos (A-C) were transferred to MATLAB 2018b as thermal image stacks, and then these images were utilized to determine each layer's temperature (B-D).

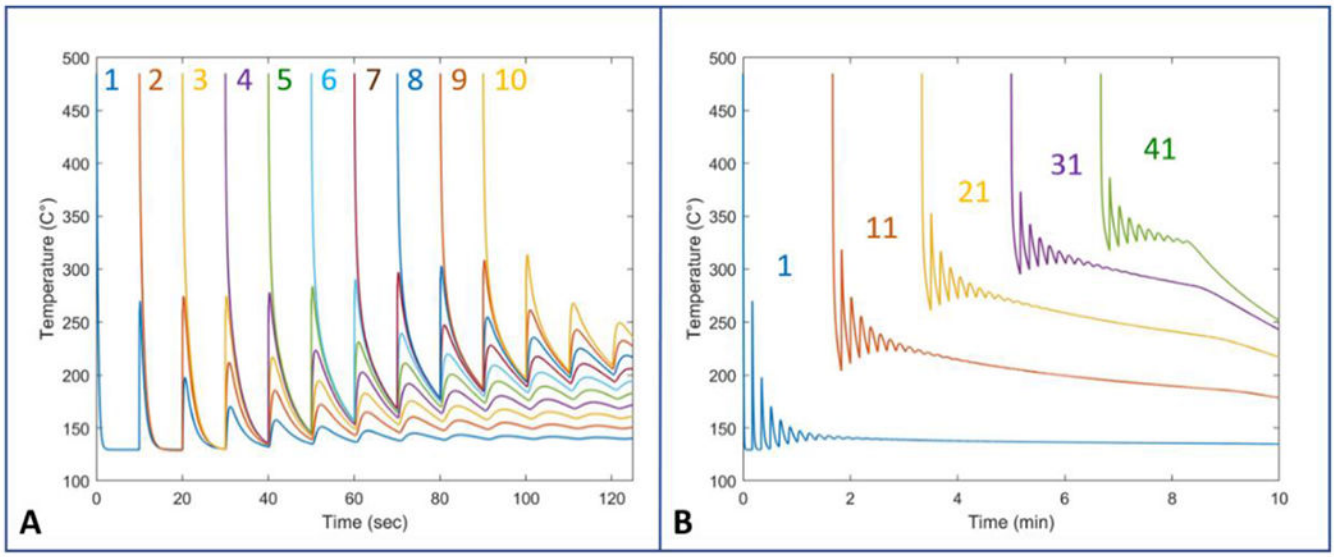


**Figure 5.**

The reheating effect of the consecutive layers can be observed from the temperature distributions of both of the first 10 layers (A), and the five layers selected from the part (B). Layer numbers are depicted next to the graphs.

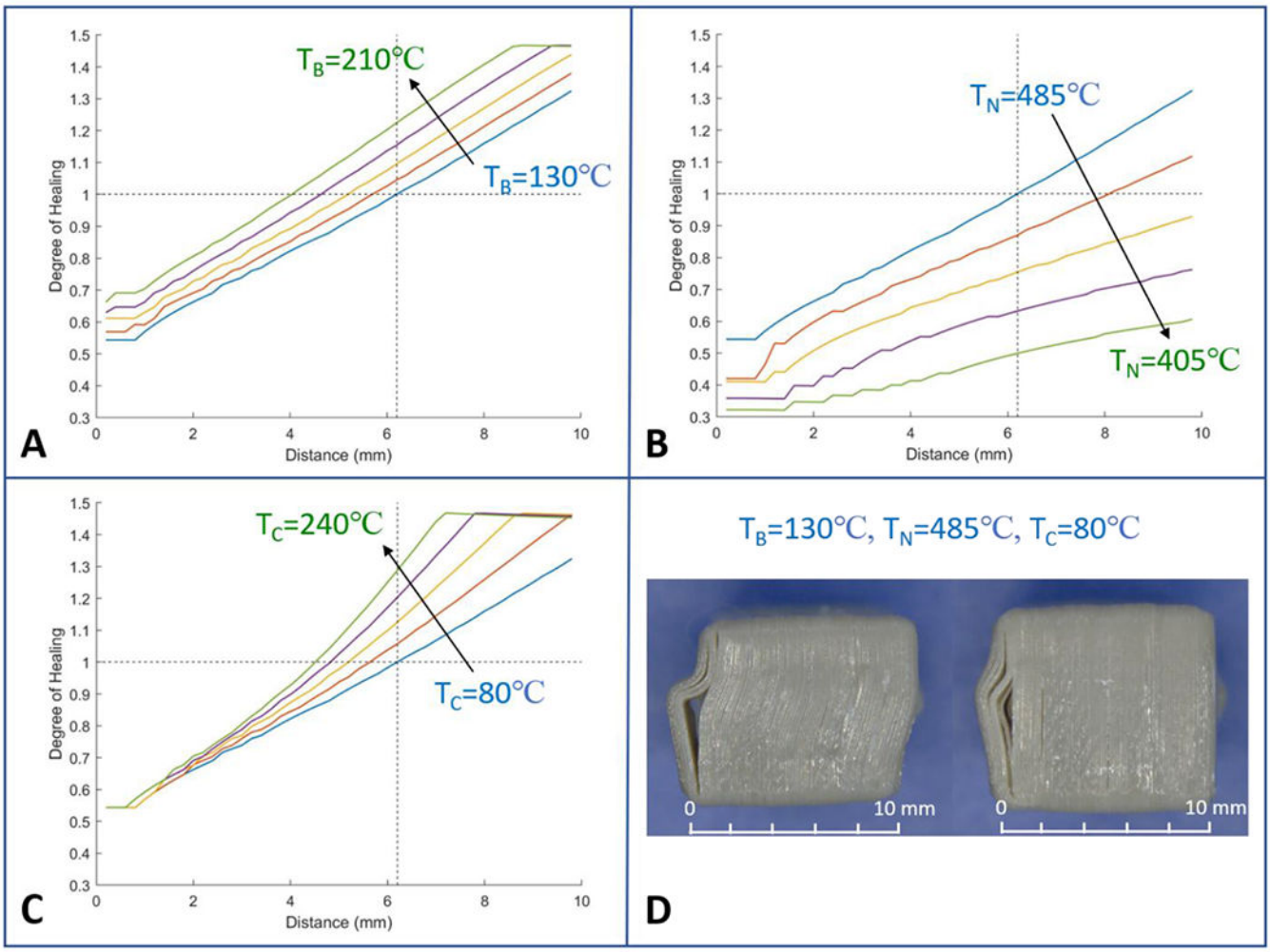


**Figure 6.**

More layers fully healed (DOH≥1) when the main FFF temperatures, print bed (A), nozzle (B), and chamber (C), were enhanced according to the model. Layer delamination failures of previously tested FFF PEEK cages under indicated temperatures support the poorer interlayer adhesion closer to the print bed (green dotted lines are showing the distance (mm) to the print bed) (D) [1].

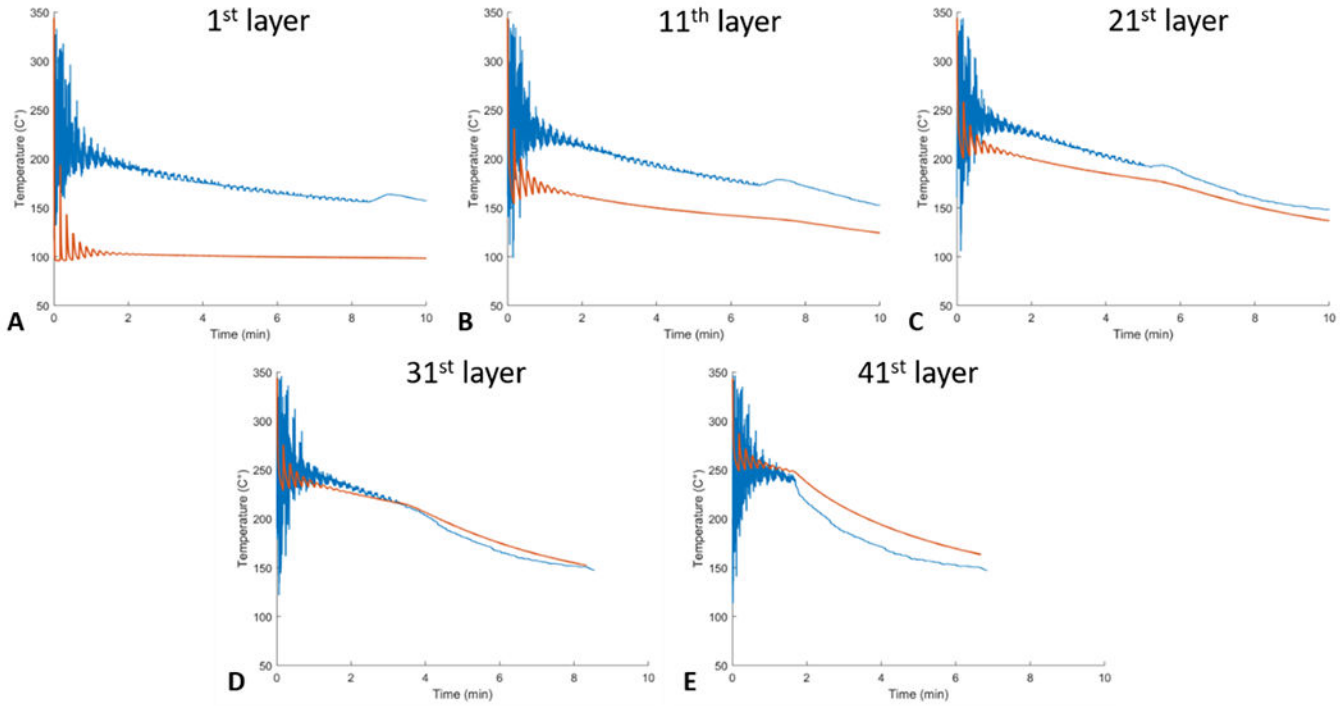


**Figure 7.**

Temperature distributions achieved from the model (red) vs experimental (blue) data were analyzed for layers of FFF PEEK cube printed in the P220 machine. As for the lower layers, conduction boundary (print bed temperature) was dominant in the model (A-B), mid-layer temperature predictions of the model and experiments were in good agreement (C-D). For upper layers, experimental layer temperatures were marginally lower than the model approximations (E).

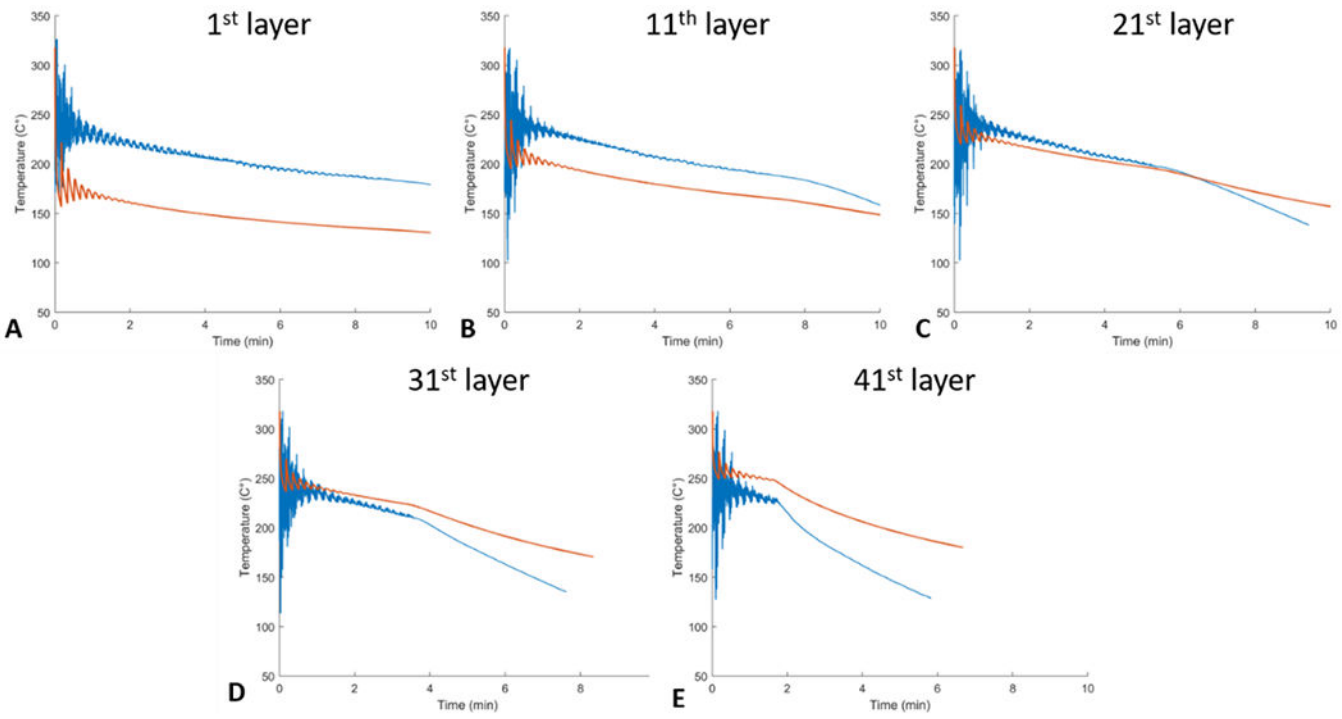


**Figure 8.**

The model (red) vs experimental (blue) temperature distributions of FFF PEEK layers were studied for the medical FFF (M220) machine. Similar to industrial (P220) machine validations, experimental layer temperatures were higher compared to the model for lower layers (A-B), whereas by the mid-layers the HTM results and the experiments were in good agreement (C). After the mid-layer, experimental layer temperatures stayed lower than the model approximations (D-E).

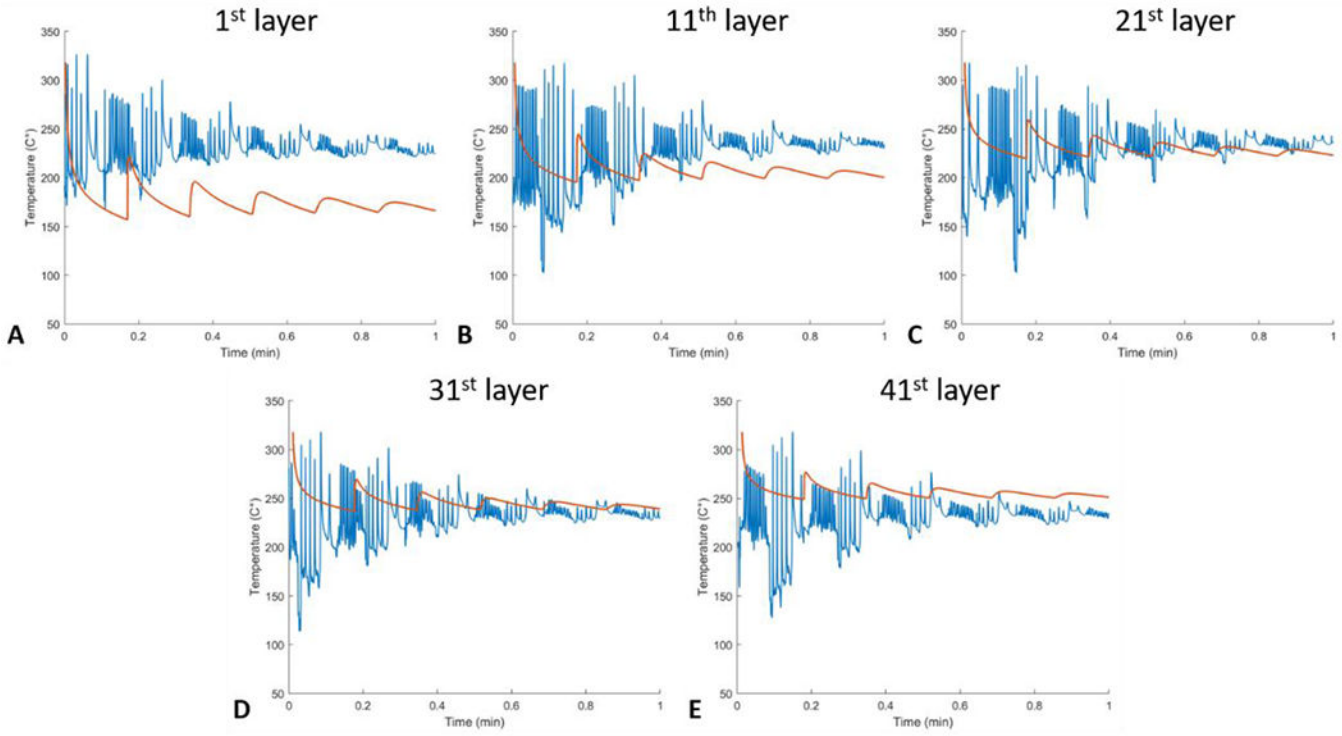


**Figure 9.**

Although the experimental layer distributions (blue) were certainly affected by the extruder while printing, the incremental convergence of the model (red) and the experiments from the beginning to the end of the FFF PEEK cube was remarkable. (medical (M220) printer results are shown here (A through E)).

**Table 1.**

Parameters used in the heat transfer model.

| Parameters | Value |
|---|---|
| Thermal conductivity, k (W/m,K) | 0.29 [23] |
| Specific heat capacity, cp (J/kg.K) | 1957 [24] |
| Density, ρ (kg/$m^3$) | 1300 [23] |
| Natural convection coefficient, h (W/$m^2$.K) | 17.5 |
| Part length, L (m) | 0.01 |
| Number of layers | 50 |
| Layer height, d (m) | 0.0002 |
| Distance between the nodes, Δx (m) | 0.0001 |
| Number of nodes, n | 101 |
| Layer deposition time, t (sec) | 10 |
| Timestep, Δt (sec) | 0.038 |
| Cooldown time (sec) | 300 |
| Initial Temperature, $T_N$ (°C) | 485 |
| Bed Temperature, $T_B$ (°C) | 130 |
| Chamber Temperature, $T_C$ (°C) | 80 |

**Table 2.**

Parameters used to calculate the natural convection coefficient ($h$).

| Parameters | Value |
|---|---|
| Fluid Temperature, $T_\infty$ (°C) | 80 |
| Surface Temperature, $T_s$ (°C) | 485 |
| Wall thickness, $L$ (m) | 0.01 |
| Fluid density, $\rho_s$ (kg/m$^3$) | 1.214 |
| Fluid kinematic viscosity, $v$ (m$^2$/s) | 1.493*10$^{-5}$ |
| Fluid specific heat capacity, $c_p$ (J/kg.K) | 1005 |
| Fluid thermal conductivity, $k$ (W/m,K) | 0.0256 |
| Fluid thermal expansion coefficient, $\beta\left(\frac{1}{\mathrm{K}}\right)$ | 3.44*10$^{-3}$ |
| Force of gravity, $g$ (m/s$^2$) | 9.81 |
| Prandtl number, $P_r$ | 0.71 |
| Grashof number, $G_r$ | 43147 |
| Average Rayleigh number, $R_a$ | 30634 |
| Average Nusselt number, $Nu_L$ | 6.97 |

**Table 3.**

FFF parameters used in this study for 2nd and 3rd generation PEEK printers.

| | 2nd Generation Printer (P220) | 3rd Generation Printer (M220) |
|---|---|---|
| **Extruder** | | |
| Nozzle Diameter | 0.4 | 0.4 |
| Extrusion Multiplier | 0.90 | 0.90 |
| Extrusion Width | 0.48 | 0.48 |
| *Ooze Control (Retraction Enabled)* | | |
| Retraction Distance (mm) | 2 | 2 |
| Retraction Speed (mm/min) | 1800 | 1800 |
| Retraction Vertical Lift | 0.15 | 0.15 |
| **Layer Settings** | | |
| Layer Height (mm) | 0.2 | 0.2 |
| Top Solid Layers | 3 | 3 |
| Bottom Solid Layers | 3 | 3 |
| Outline/Perimeter Shells | 3 | 3 |
| *First Layer Setting* | | |
| 1st Layer Height | 100% Height | 100% Height |
| 1st Layer Width | 100% Width | 100% Width |
| 1st Layer Speed | 40% | 40% |
| **Additions (Skirt/Brim)** | | |
| Use Skirt/Brim | Enabled | Enabled |
| Skirt Layers | 1 | 2 |
| Skirt Offset from Part (mm) | 0.00 | 1.00 |
| Skirt Outlines | 18 | 1 |
| Use Raft | Disabled | Enabled |
| Raft Base Layers | - | 3 |
| Raft Base Layer Height (mm) | - | 0.7 0.6 0.5 |
| Raft Base Layer Speed (mm/min) | - | 200 |
| Raft Interface Layers (mm) | - | 3 |
| Raft Interface Layer Height (mm) | - | 0.2 |
| Raft Interface Layer Speed (mm/min) | - | 2000 |
| Raft Interface Infill | - | 100% |
| Raft Offset from Part (mm) | - | -0.1 |
| **Infill Settings** | | |
| Internal Fill Pattern | Rectilinear | Rectilinear |
| External Fill Pattern | Rectilinear | Rectilinear |
| Interior Fill Percentage | 100% | 100% |

| | 2nd Generation Printer (P220) | 3rd Generation Printer (M220) |
|---|---|---|
| Outline Overlap | 50% | 50% |
| Infill Extrusion Width | 100% | 90% |
| Minimum Infill Length (mm) | 5 | 5 |
| **Temperature Settings** | | |
| Bed Temperature (°C) | 130 | 180 (Air Flow) |
| Nozzle Temperature(°C) | 440 | 440 |
| **Speed Settings** | | |
| Default Printing Speed (mm/min) | 2000 | 2000 |
| Outline Underspeed | 40% | 40% |
| Solid Infill Underspeed | 80% | 80% |
| X/Y Axis Movement Speed (mm/min) | 4800 | 4800 |
| Z Axis Movement Speed (mm/min) | 1000 | 1000 |
| **Other** | | |
| Build Volume ($mm^3$) | 205x155x150 | 130x130x130 |
| Filament Diameter (mm) | 1.75 | 1.75 |

**Table 4.**

Theoretical DOH measurements of interlayers under different temperature conditions via the HT-based DOH model.

| Bed Temperature ($T_B$, °C) | Nozzle Temperature ($T_N$, °C) | Chamber Temperature ($T_C$, °C) | Degree of Healing (DOH) | | | Interlayers with DOH<1 | Convection Coefficient (h) | Time Step (Δt, sec) |
|---|---|---|---|---|---|---|---|---|
| | | | Min | Max | Mean | | | |
| 130 | 485 | 80 | 0.54 | 1.32 | 0.91 | 30 | 17.5 | 0.038 |
| 150 | 485 | 80 | 0.57 | 1.38 | 0.95 | 28 | 17.5 | 0.038 |
| 170 | 485 | 80 | 0.61 | 1.44 | 0.99 | 25 | 17.5 | 0.038 |
| 190 | 485 | 80 | 0.63 | 1.47 | 1.05 | 23 | 17.5 | 0.038 |
| 210 | 485 | 80 | 0.66 | 1.47 | 1.10 | 20 | 17.5 | 0.038 |
| 130 | 465 | 80 | 0.42 | 1.12 | 0.79 | 40 | 17.5 | 0.038 |
| 130 | 445 | 80 | 0.41 | 0.93 | 0.68 | 49 | 17.5 | 0.025 |
| 130 | 425 | 80 | 0.36 | 0.76 | 0.57 | 49 | 17.5 | 0.025 |
| 130 | 405 | 80 | 0.32 | 0.61 | 0.45 | 49 | 17.5 | 0.013 |
| 130 | 485 | 120 | 0.54 | 1.46 | 0.96 | 28 | 16.9 | 0.038 |
| 130 | 485 | 160 | 0.54 | 1.47 | 1.00 | 25 | 16.13 | 0.038 |
| 130 | 485 | 200 | 0.54 | 1.47 | 1.04 | 24 | 15.26 | 0.038 |
| 130 | 485 | 240 | 0.54 | 1.47 | 1.07 | 22 | 14.2 | 0.038 |

**Table 5.**

Parameters used in model validation for both generations of FFF printers.

| Parameters | 2nd Generation Printer (P220) | 3rd Generation Printer (M220) |
|---|---|---|
| Thermal conductivity, k (W/m,K) | 0.29 | 0.29 |
| Specific heat capacity, cp (J/kg.K) | 1957 | 1957 |
| Density, ρ ($kg/m^3$) | 1300 | 1300 |
| Natural convection coefficient, h ($W/m^2$. K) | 14.9 | 14.9 |
| Part length, L (m) | 0.01 | 0.012 |
| Number of layers | 50 | 62 |
| Layer height, d (m) | 0.0002 | 0.0002 |
| Distance between the nodes, Δx (m) | 0.0001 | 0.0001 |
| Number of nodes, n | 101 | 125 |
| Layer deposition time, t (sec) | 10 | 10 |
| Time step, Δt (sec) | 0.033 | 0.033 |
| Cool down time (sec) | 300 | 300 |
| Initial Temperature, $T_N$ (°C) | 344 | 318 |
| Bed Temperature, $T_B$ (°C) | 95 | 91 |
| Chamber Temperature, $T_C$ (°C) | 213 | 215 |